Electro–optical tunable waveguide embedded multiscan Bragg gratings in lithium niobate by direct femtosecond laser writing

Sebastian Kroesen,* Wolfgang Horn, Jörg Imbrock, and Cornelia Denz

Institute of Applied Physics and Center for Nonlinear Science, University of Muenster, Corrensstr. 2-4, 48149 Muenster, Germany

*s.kroesen@wwu.de

Abstract: We report on the monolithic integration of waveguide embedded, electro–optical tunable Bragg gratings in lithium niobate fabricated by direct femtosecond laser writing. The hybrid design that consists of a circular type-II waveguide and a multiscan type-I Bragg grating exhibits low loss ordinary and extraordinary polarized guiding as well as narrowband reflections in the c-band of optical communications. High bandwidth tunability of more than a peak width and nearly preserved electro–optic coefficients of $r_{13} = 7.59\,\mathrm{pm\,V^{-1}}$ and $r_{33} = 23.21\,\mathrm{pm\,V^{-1}}$ are demonstrated.

OCIS codes: (140.3390) Laser materials processing; (160.3730) Lithium niobate; (230.3120) Integrated optics devices; (230.7370) Waveguides; (230.1480) Bragg reflectors.

References and links

1. K. M. Davis, K. Miura, N. Sugimoto, and K. Hirao, "Writing waveguides in glass with a femtosecond laser," Opt. Lett. **21**, 1729–1731 (1996).
2. R. R. Gattass and E. Mazur, "Femtosecond laser micromachining in transparent materials," Nat. Photonics **2**, 219–225 (2008).
3. G. Della Valle, R. Osellame, and P. Laporta, "Micromachining of photonic devices by femtosecond laser pulses," J. Opt. A: Pure Appl. Opt. **11**, 013001 (2009).
4. R. Osellame, G. Cerullo, and R. Ramponi, *Femtosecond Laser Micromachining: Photonic and Microfluidic Devices in Transparent Materials* (Springer, 2012).
5. F. Chen and J. R. V. de Aldana, "Optical waveguides in crystalline dielectric materials produced by femtosecond-laser micromachining," Laser Photonics Rev. **8**, 251–275 (2014).
6. J. Thomas, M. Heinrich, P. Zeil, V. Hilbert, K. Rademaker, R. Riedel, S. Ringleb, C. Dubs, J. Ruske, S. Nolte, and A. Tünnermann, "Laser direct writing: Enabling monolithic and hybrid integrated solutions on the lithium niobate platform," Phys. Status Solidi A **208**, 276–283 (2011).
7. R. S. Weis and T. K. Gaylord, "Lithium niobate: Summary of physical properties and crystal structure," Appl. Phys. A **37**, 191–203 (1985).
8. J. Burghoff, S. Nolte, and A. Tünnermann, "Origins of waveguiding in femtosecond laser-structured $LiNbO_3$," Appl. Phys. A **89**, 127–132 (2007).
9. A. Rdenas, A. H. Nejadmalayeri, D. Jaque, and P. Herman, "Confocal raman imaging of optical waveguides in $LiNbO_3$ fabricated by ultrafast high-repetition rate laser-writing," Opt. Express **16**, 13979–13989 (2008).
10. A. Rodenas, L. M. Maestro, M. Ramirez, G. A. Torchia, L. Roso, F. Chen, and D. Jaque, "Anisotropic lattice changes in femtosecond laser inscribed nd3+:MgO:$LiNbO_3$ optical waveguides," J. Appl. Phys. **106**, 013110 (2009).
11. J. Burghoff, H. Hartung, S. Nolte, and A. Tünnermann, "Structural properties of femtosecond laser-induced modifications in $LiNbO_3$," Appl. Phys. A **86**, 165–170 (2006).
12. J. Burghoff, C. Grebing, S. Nolte, and A. Tünnermann, "Efficient frequency doubling in femtosecond laser-written waveguides in lithium niobate," Appl. Phys. Lett. **89**, 081108 (2006).

#214850 - $15.00 USD Received 26 Jun 2014; revised 15 Aug 2014; accepted 21 Aug 2014; published 17 Sep 2014

13. J. Burghoff, C. Grebing, S. Nolte, and A. Tünnermann, "Waveguides in lithium niobate fabricated by focused ultrashort laser pulses," Appl. Surf. Sci. **253**, 7899–7902 (2007).
14. W. Horn, S. Kroesen, J. Herrmann, J. Imbrock, and C. Denz, "Electro-optical tunable waveguide Bragg gratings in lithium niobate induced by femtosecond laser writing," Opt. Express **20**, 26922–26928 (2012).
15. R. He, Q. An, Y. Jia, G. R. Castillo-Vega, J. R. Vzquez de Aldana, and F. Chen, "Femtosecond laser micromachining of lithium niobate depressed cladding waveguides," Opt. Mater. Express **3**, 1378–1384 (2013).
16. A. G. Okhrimchuk, A. V. Shestakov, I. Khrushchev, and J. Mitchell, "Depressed cladding, buried waveguide laser formed in a YAG:Nd^{3+} crystal by femtosecond laser writing," Opt. Lett. **30**, 2248–2250 (2005).
17. H. Liu, Y. Jia, J. R. Vzquez de Aldana, D. Jaque, and F. Chen, "Femtosecond laser inscribed cladding waveguides in Nd:YAG ceramics: Fabrication, fluorescence imaging and laser performance," Opt. Express **20**, 18620–18629 (2012).
18. G. Salamu, F. Jipa, M. Zamfirescu, and N. Pavel, "Laser emission from diode-pumped Nd:YAG ceramic waveguide lasers realized by direct femtosecond-laser writing technique," Opt. Express **22**, 5177–5182 (2014).
19. G. Salamu, F. Jipa, M. Zamfirescu, and N. Pavel, "Cladding waveguides realized in Nd:YAG ceramic by direct femtosecond-laser writing with a helical movement technique," Opt. Mater. Express **4**, 790–797 (2014).
20. Y. Nasu, M. Kohtoku, and Y. Hibino, "Low-loss waveguides written with a femtosecond laser for flexible interconnection in a planar light-wave circuit," Opt. Lett. **30**, 723–725 (2005).
21. R. Thomson, H. Bookey, N. Psaila, S. Campbell, D. Reid, S. Shen, A. Jha, and A. Kar, "Internal gain from an erbium-doped oxyfluoride-silicate glass waveguide fabricated using femtosecond waveguide inscription," IEEE Photon. Technol. Lett. **18**, 1515–1517 (2006).
22. G. Brown, R. R. Thomson, A. K. Kar, N. D. Psaila, and H. T. Bookey, "Ultrafast laser inscription of Bragg-grating waveguides using the multiscan technique," Opt. Lett. **37**, 491–493 (2012).
23. S. Gross, M. Ams, D. G. Lancaster, T. M. Monro, A. Fuerbach, and M. J. Withford, "Femtosecond direct-write überstructure waveguide Bragg gratings in ZBLAN," Opt. Lett. **37**, 3999–4001 (2012).
24. A. Okhrimchuk, V. Mezentsev, A. Shestakov, and I. Bennion, "Low loss depressed cladding waveguide inscribed in YAG:Nd single crystal by femtosecond laser pulses," Opt. Express **20**, 3832–3843 (2012).
25. Y. Liao, J. Xu, Y. Cheng, Z. Zhou, F. He, H. Sun, J. Song, X. Wang, Z. Xu, K. Sugioka, and K. Midorikawa, "Electro-optic integration of embedded electrodes and waveguides in $LiNbO_3$ using a femtosecond laser," Opt. Lett. **33**, 2281–2283 (2008).
26. T. Erdogan, "Fiber grating spectra," J. Lightwave Technol. **15**, 1277–1294 (1997).
27. Z. Toroker and M. Horowitz, "Optimized split-step method for modeling nonlinear pulse propagation in fiber Bragg gratings," J. Opt. Soc. Am. B **25**, 448–457 (2008).
28. A. Benayas, W. F. Silva, C. Jacinto, E. Cantelar, J. Lamela, F. Jaque, J. R. Vzquez de Aldana, G. A. Torchia, L. Roso, A. A. Kaminskii, and D. Jaque, "Thermally resistant waveguides fabricated in Nd:YAG ceramics by crossing femtosecond damage filaments," Opt. Lett. **35**, 330–332 (2010).
29. S. H. Lee, S. H. Kim, K. H. Kim, M. H. Lee, and E.-H. Lee, "A novel method for measuring continuous dispersion spectrum of electro-optic coefficients of nonlinear materials," Opt. Express **17**, 9828–9833 (2009).

1. Introduction

Waveguides and functional optical devices such as modulators, amplifiers, frequency converters or narrowband filters are fundamental components of optical communications and integrated optics. Similar to their electronic counterparts, integrated optical elements provide miniaturized feature size and a multitude of passive and active elements can be employed to realize complex optical circuits. In addition to common lithographic techniques such as ion in–diffusion or ion implantation, direct femtosecond laser writing is nowadays recognized as a versatile tool to inscribe waveguide structures into various materials including glasses, crystals, and ceramics [1–4]. The technique relies on a strongly localized refractive index modification by nonlinear absorption inside the host material. By translating the host material with respect to the writing beam, arbitrary three–dimensional refractive index structures on a sub-micrometer length scale can be realized.

The essential property for direct laser writing schemes in general is the induced refractive index change, which depends on inscription parameters such as pulse duration, pulse energy, repetition rate, and numerical aperture of the employed microscope objective, but most importantly on the structural change of the material induced by the intense writing beam. For integration of functional optical devices, it is indispensable to inscribe waveguide structures, couplers, and gratings into nonlinear optical materials to exploit their inherent reconfigurability, adaptiv-

#214850 - $15.00 USD Received 26 Jun 2014; revised 15 Aug 2014; accepted 21 Aug 2014; published 17 Sep 2014

ity and tunability [5, 6]. Lithium niobate ($LiNbO_3$) is a well–known standard platform which is widely used in optoelectronics due to its large transmission window and excellent nonlinear properties [7]. However, in contrast to some specific isotropic materials such as fused silica, where a homogeneous refractive index change inside the focal volume of the writing beam can be achieved, the crystallographic structure of $LiNbO_3$ leads to a strongly anisotropic behavior, thus more elaborate writing geometries are required to achieve symmetric guiding.

The physical origin of the refractive index modulation in lithium niobate is nontrivial and has been discussed by various authors (e. g. [8–10] and therein). We follow the most common classification of type-I and type-II material modifications, where we focus on the low–repetition rate regime ($f_{rep} \leq 250\,kHz$). In the first case, an increased refractive index is observed in the irradiated regions. Typically, type-I structures are obtained for very low laser fluences, and the induced refractive index modulation can be completely removed by thermal annealing [11–13]. The latter case obtained for higher laser fluences corresponds to the creation of an amorphous filament and subsequent reduction of the refractive index. The guiding properties of these type-II structures are determined by the stress field distribution imposed on the crystal. In general, both types of refractive index modulation are strongly anisotropic and the nonlinear coefficients of the processed material are not necessarily preserved [11, 14], which is a bottleneck for efficient frequency conversion and signal processing.

Most recently, two–dimensional circular waveguide designs referred to as depressed cladding–, or type-III waveguides have been proposed that provide nearly balanced guidance along both input polarizations [5, 15]. These structures have attracted a lot of attention because they allow efficient waveguide lasers in active materials by direct femtosecond laser writing [16–19]. With respect to integration of functional optical elements, it is of high importance to apply these approaches to lithium niobate to achieve well confined, low loss guiding. Based on these high quality waveguide structures, more complex functionality such as integrated waveguide embedded Bragg gratings (WBG) which are widely used for filtering applications, can be realized. Although the crystallographic properties complicate direct write approaches, the outstanding nonlinear response, fast electro–optic tunability and the possibility to fabricate all–integrated optical circuits based on $LiNbO_3$ are worthwhile to investigate new writing schemes and geometries. In previous experiments it was shown that the guiding lines of a rather simple double–line configuration can be modulated periodically to realized waveguide Bragg gratings [14]. However, the structure was unable to support waveguiding of extraordinary polarized light, and the scattering loss induced by the periodic modulation was excessive, thus limiting its applications.

In this contribution, we overcome these limitations implementing a novel, hybrid type-I/II design. A type-II waveguide geometry is presented that provides low loss, symmetric guiding with a superior mode fidelity, which is mandatory to access features based on the largest electro–optic coefficient r_{33} for extraordinary polarization. Type-I Bragg gratings are inscribed into the waveguide core using the multiscan technique [20–23]. Moreover, we demonstrate that the structure provides high bandwidth spectral tuning of more than a peak width and nearly preserved electro–optic coefficients.

2. Monolithic integration of waveguide embedded Bragg gratings

The inscription setup is based on an Ytterbium–doped Potassium Gadolinium Tungstate (Yb:KGW) femtosecond laser system with up to 2 mJ pulse energy at $\lambda = 1028\,nm$ central wavelength, and a three–dimensional translation stage with nanometer precision as illustrated in Fig. 1(a). The repetition rate of the laser system is adjustable over a large range reaching from single shot operation to 600 kHz. A pulse duration of approximately 190 fs is used for all experiments. Since the proposed hybrid type-I / II structures require precisely calibrated pulse

#214850 - $15.00 USD Received 26 Jun 2014; revised 15 Aug 2014; accepted 21 Aug 2014; published 17 Sep 2014

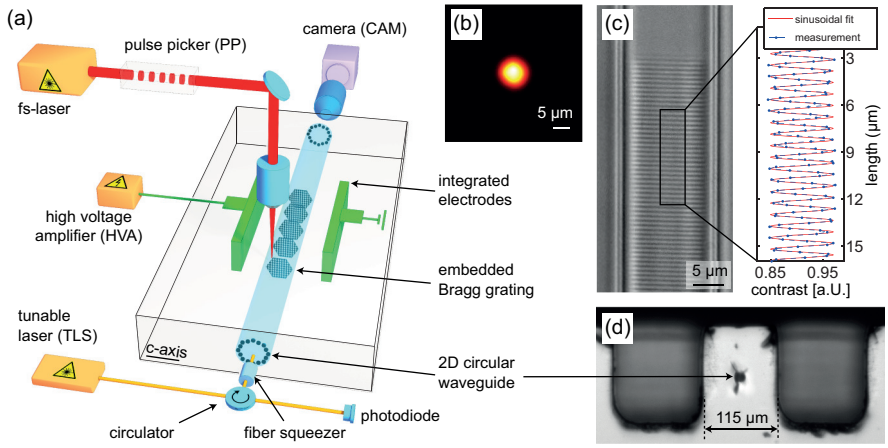

Fig. 1. (a) Schematic of the experimental setup for direct integration and characterization of waveguide embedded Bragg gratings (WBG) in $LiNbO_3$. TLS: tunable laser source; PP: pulse picker, CAM: camera, HVA: high voltage amplifier. (b) Extraordinary polarized mode of a circular waveguide structure with a diameter of 15 µm. (c) Top view of the multiscan Bragg grating with a period of $\Lambda = 704$ nm, where the upper and lower waveguide lines are omitted for clear imaging. (d) Polished cross section of a WBG with integrated electrodes.

energies from a few nanojoules to hundreds of nanojoules, an interchangeable set of neutral density filers in combination with a half wave plate and a polarizing beam splitter is employed. We use commercially available x–cut lithium niobate wafers with a thickness of 500 µm, which are cut into 10×10 mm^2 samples and subsequently polished to optical quality to ensure efficient coupling. The writing laser beam is focused at a depth of 100 µm below the surface of the substrate by a $100\times$ microscope objective with a numerical aperture of NA $= 0.8$, and the polarization is aligned parallel to the waveguide direction. As indicated in the schematic, the waveguide direction is oriented perpendicular to the crystallographic c–axis. This configuration allows the unique possibility for low operating voltages by narrow–spaced integrated electrodes, and at the same time high nonlinear response addressing the largest electro–optical coefficient of $LiNbO_3$ for extraordinary polarized probe light.

Waveguides with a permanent, high contrast refractive index profiles can be created for a large range of parameters. Basic structures consisting of less than 10 individual lines cf. Figs. 2(a1)–2(c1) are inscribed with pulse energies from 200 nJ to 750 nJ, which is associated with type-II material modifications. For multi–line geometries such as circular and depressed cladding waveguides [5, 16, 24] with a significantly higher number of tracks, lower pulse energies of 50 nJ to 125 nJ are employed (Figs. 2(d1) and 2(e1)). A vertical line spacing (or diameter for circular structures) of 8 µm to 20 µm was found to be best suited for single–mode transmission in the near–infrared. To facilitate short inscription durations even for high–resolution circular waveguides, the interrelated parameters translation velocity of the linear stage and repetition rate of the laser system (laser shots per unit distance) are maximized for a fixed pulse energy. In our experimental setup, a translation velocity of up to 8 mm s^{-1} at 100 kHz repetition rate could be realized without degradation of the waveguide power transmission and modal properties.

Second–order Bragg gratings with a period of $\Lambda = 704$ nm have been inscribed using a mul-

#214850 - $15.00 USD Received 26 Jun 2014; revised 15 Aug 2014; accepted 21 Aug 2014; published 17 Sep 2014

tiscan technique [23]. In contrast to direct point–by–point integration of strong type-II gratings [14], where the periodic modulation is achieved indirectly by the outer waveguide lines, the entire core volume of the waveguide is successively scanned and periodically modified using position–locked pulse firing with high transverse resolution and low pulse energies. Figure 1(c) shows the top view of such a multiscan Bragg grating, where the upper and lower waveguide lines are omitted for clear imaging. The unprocessed material and the smooth periodic modulation are clearly visible. The major advantage with respect to point–by–point schemes is the possibility to apply arbitrary modulation functions e. g. varying duty cycle or even aperiodic sequences. Moreover, this method is independent of deviations of the translation velocity and therefore less sensitive to perturbations. To improve the position accuracy of the linear stage a translation velocity of $0.3\,\mathrm{mm\,s^{-1}}$ is employed with a reduced repetition rate of 10 kHz. Gratings were also successfully inscribed at higher repetition rates, however the spectral response was impure and the repeatability was compromised, which is attributed to technical limitations. A transverse multiscan resolution of 300 nm in horizontal, and 700 nm in vertical direction is used, respectively.

Finally, integrated electrodes are fabricated by femtosecond material ablation [25]. The total depth of the electrodes is matched to the fabrication depth of the WBGs to ensure a uniform electric field distribution along the Bragg grating (cf. Fig. 1(d)). Subsequently, the grooves are filled with conductive silver, insulated to avoid voltage breakdown and connected to a high voltage amplifier (HVA). An electrode distance of $\mathrm{d} = 115\,\mu\mathrm{m}$ with parallel surfaces is realized without any derogation to the waveguiding properties.

Characterization of the inscribed WBGs is performed using a tunable laser source (TLS) in a typical fiber–coupling arrangement. The cleaved fiber is coupled to the substrate after passing through a circulator, which is employed to analyze the reflection properties of the Bragg gratings. The power reference is obtained by coupling the fiber to a high reflective dielectric mirror. The near–field mode profile at the exit facet is imaged onto an InGaAs camera (CAM) (cf. Fig. 1(b)). To investigate linear ordinary-, and extraordinary polarization, a fiber squeezer is used in combination with a polarizing beam splitter in front of the camera. Insertion loss measurements are also conducted for all presented waveguide configurations employing a calibrated detector.

3. Waveguide characteristics

To investigate and optimize the guiding properties, a series of different waveguide geometries referred to as double–, quad–, rectangular–, circular– and closed–circular waveguide are fabricated on a single 10 mm long sample. Figures 2(a1)–2(e1) show the corresponding optical microscope images of the polished coupling facet. The mode profiles and insertion loss (including Fresnel reflections, coupling losses and propagation loss) for ordinary (s) and extraordinary (p) polarization are shown in the *second–*, and *third row*, respectively. All images are scaled to the maximum power transmission obtained for the closed–circular waveguide and ordinary polarization.

The central double–lines in Figs. 2(a1)–2(c1) are inscribed with a pulse energy of 600 nJ whereas 225 nJ is used for the upper and lower lines (Figs. 2(b1) and 2(c1)). The vertical line spacing or diameter is 15 µm for all presented structures. Depending on the geometry, slightly varying pulse energies could be used to optimize the power transmission, however a fixed set of parameters is used for better comparability. It can be clearly seen that the power transmission, particularly for p–polarized probe light, significantly increases by altering the geometry adding two or more lines in vertical direction. For instance, the insertion loss of the quad structure is improved by approximately 4 dB with respect to the basic double–line configuration. This simple structural change can be of practical use for low repetition rate systems, where multiple

#214850 - $15.00 USD Received 26 Jun 2014; revised 15 Aug 2014; accepted 21 Aug 2014; published 17 Sep 2014

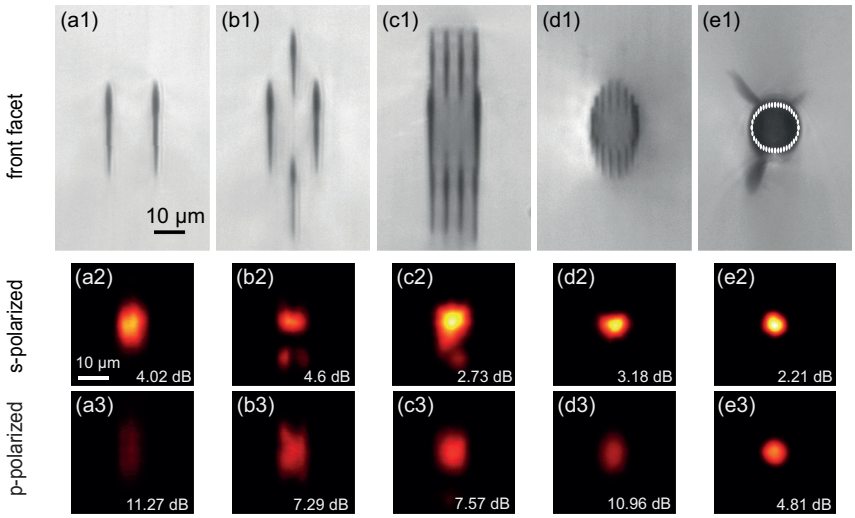

Fig. 2. *(first row)* Optical microscope images of the front facet of different two–dimensional waveguide structures in lithium niobate referred to as (a1) double–, (b1) quad–, (c1) rectangular–, (d1) circular– and (e1) closed–circular waveguide. Corresponding mode profiles and insertion loss for *(second row)* ordinary-, and *(third row)* extraordinary polarization at $\lambda = 1.55\,\mu$m, respectively. Symmetric single mode transmission with an insertion loss of 4.81 dB and nearly perfect mode–circularity of 99.5 % is achieved for the proposed closed–circular waveguide design and extraordinary polarization.

tracks cause excessive inscription durations and extraordinary guidance is required. Although the modal properties of the quad structure are satisfactory in most cases, the rectangular structure tends to show multimode behavior, and it is difficult to achieve symmetric guiding for both polarization states within one set of parameters. As shown in Figs. 2(c2) and 2(c3) a line separation of 3.5 µm leads to moderate insertion loss and an acceptable mode–profile for p–polarized light, while s–polarized light is multimode, thus many different coupling states are possible. Moreover, slight changes in the vertical distance or deviations of the employed pulse energy strongly affect the modal properties making it very challenging to determine and repeat inscription parameters.

Considerably improved performance is observed for circular waveguide structures, where two different types are investigated. In the first configuration referred to as depressed–cladding waveguide (or type-III waveguide [5]), the waveguide is composed of multiple filaments arranged in that way that an aperture of circular shape remains unprocessed as shown in Fig. 2(d1). The individual lines are inscribed with a line–spacing of 1.5 µm and 125 nJ pulse energy. These waveguides exhibit good power transmission and the diameter can be adapted to achieve single–mode propagation at mid–infrared spectral regions [15]. Although low insertion loss of 0.5 dB at $\lambda = 1064\,$nm was reported for a waveguide with a diameter of 50 µm [15], the waveguide was highly multimode and low insertion loss was only achieved for a waveguide direction along the c–axis (both polarizations are ordinary polarized). Particularly for inscription of waveguide embedded Bragg gratings single–mode propagation is mandatory to suppress cladding modes and to realize high fidelity reflection spectra. In case of the depressed–cladding waveguides, this could only be achieved by reducing the diameter to less than 18 µm. However, symmetric guiding was still not possible. The structure could be either optimized for ordinary–, or extraordinary polarization. The best compromise is shown in Figs. 2(d2) and 2(d3), where a slightly elliptical mode with an insertion loss of 10.96 dB is obtained for p–polarization, while

#214850 - $15.00 USD Received 26 Jun 2014; revised 15 Aug 2014; accepted 21 Aug 2014; published 17 Sep 2014

the transmission for s–polarized light is higher. A further increase of the employed pulse energy leads to multimode operation for s–polarized light and an improved power transmission for p–polarized light.

We developed a waveguide configuration that provides symmetric single–mode propagation for ordinary–, and extraordinary input polarization. The line spacing is reduced to 750 nm so that the individual lines form a continuous circular material modification as shown in Fig. 2(e1). Since the consecutively inscribed lines are not distinguishable due to their high spatial overlap, their addressed position and size is indicated by the white elongated spots. The structure, which is referred to as *closed–circular*, is similar to those realized by Salamu et al. [19]. However, the helical writing scheme cannot be employed since waveguide embedded Bragg gratings require a transverse writing geometry in a bottom–up–scheme. It can be seen that the dense material modifications lead to cracks outside the central guiding area and the waveguide aperture with a diameter of 12 µm appears dark in the phase–contrast image. In contrast to this visual impression, the structure provides superior guiding and modal characteristics indicating that the core region remains unaffected besides the strong induced stress field. A mode circularity of 99.5 % and 4.81 dB insertion loss for extraordinary polarization is achieved using a pulse energy of 65 nJ as shown in Fig. 2(e3). The presented closed–circular waveguide exhibits pure single–mode propagation for both, ordinary and extraordinary polarized light. With respect to depressed cladding waveguides particularly the ratio of ordinary and extraordinary insertion loss as well as modal properties are significantly improved. Hence these parameters are used for all further experiments and an average propagation loss of (1.1 - 1.6) dB cm^{-1} of ordinary–, and (3.0 - 3.8) dB cm^{-1} for extraordinary polarization was obtained for different experimental series (samples) and waveguide lengths, respectively.

4. Spectral properties of embedded Bragg gratings

To analyze coupling strength and spectral properties of embedded Bragg gratings, different series of second–order WBGs with increasing grating strength (pulse energy employed for the multiscan sequence) are inscribed. Series–1 consists of ten 0.5 mm long gratings with pulse energies reaching from 3.6 nJ to 4.05 nJ. Whereas slightly lower pulse energies of 3.4 nJ to 3.85 nJ are used for series–2 (grating length 1 mm). The individual Bragg gratings are embedded into a closed–circular waveguide (L = 10 mm) with an inset of 1 mm with respect to the front facet. The waveguide parameters are equal to those given in Fig. 2(e1). The selected pulse energies cover the ideal type-I operation window that reaches from no detectable refractive index modulation to a starting type-II filamentation process.

Figures 3(a) and 3(b) show the power reflection spectra of a particular WBG inscribed with a pulse energy of 3.65 nJ. A power reflection of approximately 30 % for (a) s–polarized, and 6 % for (b) p–polarized light is achieved. The wavelength offset of the central Bragg reflection maxima ($\lambda_o - \lambda_e = 49.77$ nm) corresponds to the birefringence of lithium niobate. Effective refractive indices of $n_o = 2.2044$ and $n_e = 2.134$ are calculated for an addressed period of $\Lambda = 707$ nm. To demonstrate the embedded character of the presented gratings and to confirm the propagation loss calculated from the power transmission, the WBG is probed from opposite sides denoted as *front–*, and *back–coupling*. It can be seen that the spectral characteristics coincide to a high degree indicating the superior quality of the presented hybrid type-I/II WBG design. We performed numerical calculations to estimate the effective refractive index modulation to be $\Delta n_o = 6.9 \times 10^{-4}$ and $\Delta n_e = 2.75 \times 10^{-4}$ with a propagation loss of $\alpha_o = 1.52$ dB cm^{-1} and $\alpha_e = 3.51$ dB cm^{-1}.

We use a split-step method based on the linear coupled mode equations [26, 27] to calculate the refractive index modulation for the entire series of WBGs as shown in Fig. 3(c). The polarization dependent coupling–, and propagation loss of each WBG is considered to fit the

#214850 - $15.00 USD Received 26 Jun 2014; revised 15 Aug 2014; accepted 21 Aug 2014; published 17 Sep 2014

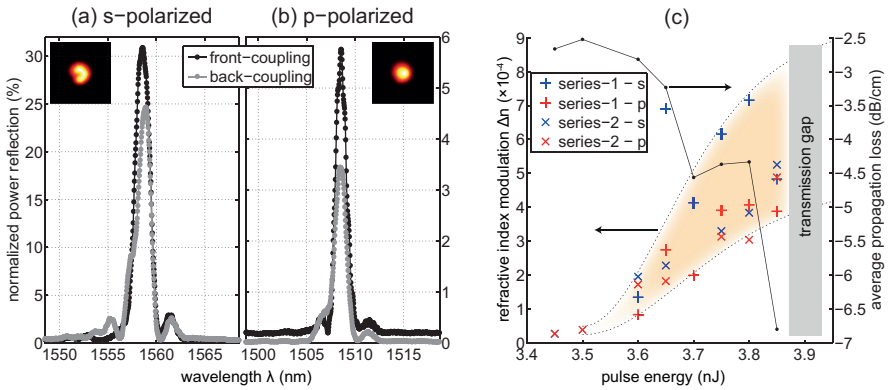

Fig. 3. Reflection spectra of a 0.5 mm long Bragg grating embedded into a 10 mm long closed–circular waveguide for (a) ordinary-, and (b) extraordinary input polarization. The embedded character is demonstrated by probing the sample from opposite sides denoted as *front–*, and *back–coupling*. (c) Calculated refractive index modulation as a function of the pulse energy used for the multiscan Bragg gratings. It can be seen that the operation window is extremely narrow and too high pulse energies cause a derogated power transmission due to the starting filamentation process.

obtained reflection spectra. It can be seen that the operation window is rather narrow and precise calibration and power stability of the writing laser system is required. Since the core volume of the waveguide is scanned approximately 300 times, the total inscription duration of a single structure with the given parameters of series–1/2 is of the order of 40 min. Consequently, even slight misalignment of the employed pulse energy or long term drift of the laser system causes a considerable change of the deposited energy, which also explains the present deviations of the coupling strength for different inscription series. The induced refractive index modulation follows a tanh–characteristic centered around 3.7 nJ within our experimental configuration. The energy threshold of the type-II filamentation process is around 3.9 nJ for the high resolution multiscan approach. As a consequence, the power transmission decreases for an increasing grating strength limiting the applicable refractive index modulation to values of $\Delta n_{o,e} < 1 \times 10^{-3}$, which is in good agreement with the typical refractive index change obtained for type-I modifications [8]. In contrast to Burghoff et al., both refractive indices are altered by the material processing. To prove that the multiscan Bragg gratings are inscribed very close to the threshold energy between type-I and type-II modifications, the presented WBGs are thermally annealed at 250 °C for 24 h. In accordance to [15], the power transmission is improved for both polarizations. The power reflection of the Bragg gratings was completely erased for pulse energies lower than 3.5 nJ, whereas the power reflection for the remaining series was only slightly reduced. Moreover, the spectral properties are improved, e. g. undesired sidelobes are cleared out and the reflection spectrum becomes more symmetric. Besides the change of the modal and spectral properties caused by the annealing procedure no deterioration of the waveguide Bragg grating performance was observed at all within a time period of several months.

Consequently, it is possible to integrate permanent, thermally stable WBGs with a reasonably high power transmission and sophisticated spectral properties by the proposed technique. Symmetric low loss single–mode propagation as well as narrowband reflections are achieved within one structure.

#214850 - $15.00 USD Received 26 Jun 2014; revised 15 Aug 2014; accepted 21 Aug 2014; published 17 Sep 2014

5. Electro–optical tuning

Nonlinear electro–optic tuning is performed for a WGB selected from the second series and an electrode distance of $d = 115\,\mu m$. The Bragg grating inscribed with a pulse energy of 3.8 nJ exhibits a reflectivity of 8 % (probing from the back–facet) and narrow $1/e^2$ width of $\Delta\lambda = 1.07\,nm$. To perform frequency tests as well as strong applied electric fields, two different high voltage amplifiers are used. A sinusoidal probe signal is applied, and the photo diodes (transmission and reflection) as well as the monitor voltage of the HVA are measured. The data acquisition is triggered by the sync–source of the high frequency generator and the spectrum is scanned by the tunable laser source (TLS) with a wavelength step size of 5 pm.

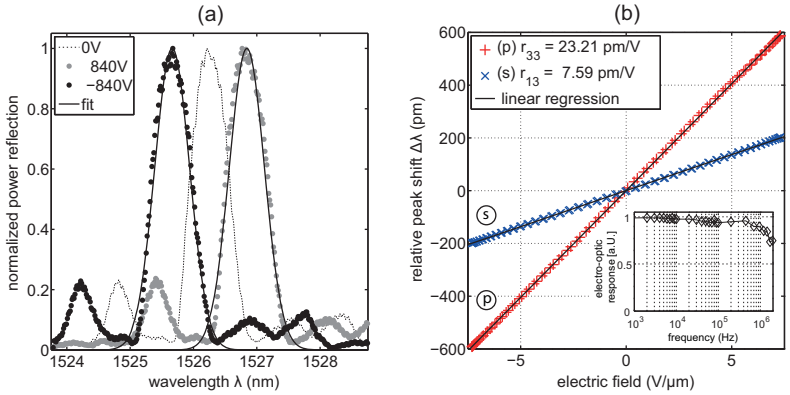

Fig. 4. Electro–optic tuning of a 1 mm long WBG. (a) A maximum spectral tuning of more than a peak width is achieved with an applied voltage of $\pm 840\,V$ for p–polarized light. The spectral characteristics are preserved to a high degree indicating a uniform field distribution and pure single–mode propagation. (b) Relative shift of the central Bragg reflection maxima for s–, (ordinary) and p–polarized light (extraordinary). Nearly preserved electro–optic coefficients of $r_{13} = 7.59\,pm\,V^{-1}$ and $r_{33} = 23.21\,pm\,V^{-1}$ are obtained with a perfectly linear response. (b-*inset*) Frequency test of the device to show high bandwidth operation.

The maximum spectral tuning at a modulation frequency of 1 kHz is shown in Fig. 4(a) where the black dotted line indicates the reference spectrum without an applied electric field. A relative peak shift of $\lambda_e' = \pm 590\,pm$ is achieved for p–polarized light with an applied voltage of $\pm 840\,V$. This demonstrates that the reflection maximum is shifted by more than a peak width without any spectral deformations indicating a uniform field distribution and pure single–mode transmission. In former experiments with basic waveguide geometries, where multiple coupling positions were possible, the reflection spectrum was deformed by the high applied electric field. For some configurations a mode splitting was observed that caused an increased reflection bandwidth or even separated reflection maxima.

The central Bragg wavelength $\lambda_{o,e}$ is shifted according to the linear Pockels effect. For second–order gratings, the Bragg equation simplifies to $\lambda'_{o,e} = (n_{o,e} + \Delta n_{NL})\Lambda$ where $\Delta n_{NL} = -0.5 n_{o,e}^3 r_{13,33} U/d$ denotes the induced nonlinear refractive index change. The electro–optic coefficients for light polarized along the principle crystallographic axis are referred to as $r_{13,33}$ and U denotes the applied voltage over a distance d. Figure 4(b) depicts the relative shift $\Delta\lambda_{o,e} = \lambda'_{o,e} - \lambda_{o,e}$ of the central Bragg reflection wavelength as a function of the electric field for both input polarizations. Assuming that the nonlinearity is the same in the low and high refractive index regions of the Bragg grating, the effective electro–optic coefficients can be calculated by the linear regression of $2\Delta\lambda_{o,e}/n_{o,e}^3\Lambda = r_{13,33}U/d$. Both traces exhibit perfectly

#214850 - $15.00 USD Received 26 Jun 2014; revised 15 Aug 2014; accepted 21 Aug 2014; published 17 Sep 2014

linear characteristics and nearly preserved electro–optic coefficients of $r_{13} = 7.59\,\mathrm{pm\,V^{-1}}$ (s–pol) and $r_{33} = 23.21\,\mathrm{pm\,V^{-1}}$ (p–pol) are obtained, which corresponds to more than 80 % of bulk lithium niobate [29]. Similar coefficients are measured for the entire series of WBGs indicating that the small reduction of the nonlinear response is a property of the waveguide rather than it is induced by the modification of the core region. Furthermore, frequency tests are performed with a modulation frequency up to 2 MHz. The normalized electro-optic response (electro–optic coefficients normalized with respect to those obtained at 1 kHz) reproduces exactly the frequency characteristics of the high voltage amplifier. Hence, the proposed scheme could in principle also be applied to higher bandwidth reducing the electrode distance and subsequently the operation voltage. We have to point out that the presented WBGs possess an unexpected low–frequency-, or DC behavior. The maximum induced wavelength shift is reduced in this case, which is most likely due to an internal electric field that compensates the external applied field to some degree. However, this effect is out of the scope of this publication. Since this effect is present only for DC–operation or frequencies lower than 10 Hz it does not hamper application of the proposed WBGs at all.

The presented experimental results on waveguide embedded Bragg gratings denote an important improvement to previously reported experiment, where an effective coefficient of $r_{\mathrm{eff}} = 3.66\,\mathrm{pm\,V^{-1}}$ was obtained for ordinary polarized light [14]. Particularly, the narrow–spaced electrodes and accessibility of the large extraordinary coefficient r_{33} are the key step towards high bandwidth applications. This work shows the first successful application of the multiscan technique in crystalline materials with sub–micrometer periods. In principle the scheme could also be applied to active materials to fabricate efficient waveguide integrated distributed feedback (DFB), distributed Bragg reflector (DBR) lasers or nonlinear frequency converters. Further investigations of the two–dimensional refractive index profile and changes induced to the lithium niobate network for instance by Raman spectroscopic methods [9] could lead to deeper understanding of the underlying processes and play an important role in the WBG design optimization.

6. Conclusion

In conclusion, second–order multiscan Bragg gratings are embedded into the core volume of a complex two–dimensional waveguide in $LiNbO_3$. The hybrid structure exhibits low loss, symmetric guiding with superior mode fidelity and narrowband reflection in the c–band of optical communications. Nearly preserved electro–optic coefficients of $r_{13} = 7.59\,\mathrm{pm\,V^{-1}}$ (s–pol) and $r_{33} = 23.21\,\mathrm{pm\,V^{-1}}$ (p–pol) facilitate spectral tuning of more than a peak width, which is a key feature for functional optical devices and high bandwidth signal processing. The proposed design paves the way to fully exploit features on nonlinearity in integrated optics by direct femtosecond laser writing.

Acknowledgments

This work was support by Deutsche Forschungsgemeinschaft and Open Access Publication Fund of University of Muenster. We specially thank TOPAG for providing the femtosecond laser system for this project.

#214850 - $15.00 USD Received 26 Jun 2014; revised 15 Aug 2014; accepted 21 Aug 2014; published 17 Sep 2014